Pergamon

Acta mater. 48 (2000) 4007–4020

Acta MATERIALIA

www.elsevier.com/locate/actamat

PREDICTING THE SIZE- AND TEMPERATURE-DEPENDENT SHAPES OF PRECIPITATES IN Al–Zn ALLOYS

S. MÜLLER[1]*, C. WOLVERTON[2], L. -W. WANG[1] and A. ZUNGER[1]
[1]National Renewable Energy Laboratory, Golden, CO 80401, USA, and [2]Ford Research Laboratory,
MD3028/SRL, Dearborn, MI 48121-2053, USA

(Received 22 February 2000; received in revised form 27 June 2000; accepted 28 June 2000)

Abstract—We study theoretically the size versus shape versus temperature relation of precipitates in Al–Zn via quantum-mechanical first-principles simulations. Our parameter-free model, based on a mixed-space cluster expansion, allows the prediction of the experimentally observed size and temperature dependences of the precipitate shape. We find that aging experiments can be explained in terms of equilibrium shapes. The precipitates change from a nearly spherical to a more ellipsoidal/hexagonal shape with increasing size and decreasing temperature. They always flatten in the [111] direction, which can be interpreted as a consequence of a mechanical instability of face-centered cubic Zn when rhombohedrally distorted along [111] and a strong anisotropy of the chemical energy. The excellent agreement between experiment and theory shows that our model can be used to quantitatively *predict* precipitate shapes and sizes. *© 2000 Acta Metallurgica Inc. Published by Elsevier Science Ltd. All rights reserved.*

Keywords: Aluminum alloys; Aging; Computer simulation; Ab initio calculation; Thermodynamics

1. INTRODUCTION

Precipitates are formed by quenching a homogeneous solid solution into a two-phase region of the phase diagram, followed by sample aging [1–3]. Coherent precipitation (i.e., with no dislocations between precipitate and matrix) often occurs when the aging temperature is below the coherent phase boundary. The identity of the phases in the two-phase region determines the geometrical and chemical properties of the precipitates. In Al–Zn, the two-phase region corresponds to elemental Al and Zn, so that precipitates formed from the Al-rich solid solution consist of only Zn atoms. In Al–Cu, the two-phase region corresponds to Al and Al_3Cu, so that the precipitate observed is a compound ([1]; for a review of the controversial results on coherent precipitation in Al–Cu, see the *Scripta Metallurgica* Viewpoint Set, edited by Gerold [4]). Precipitates are important for a few reasons. (1) In metal alloys, they act as obstacles for dislocations. This effect is responsible for strengthening and hardening of metal alloys. Since *coherent* precipitates involve no dislocations between precipitate and matrix, they are very effective at strengthening in alloys [1–3]. (2) In semiconductor alloys, precipitates lead to profound changes in their optical properties [5, 6], including changes of band gaps and polarization.

The interesting feature of the Al–Zn system is the existence of a solid solution over a broad temperature and concentration regime [7–10] (indeed, of all the elements, Zn has the largest solid solubility in Al with a maximum of 66.4 at.% Zn [11]). Since Al–Zn belongs to the class of heat-treatable alloys, knowledge of the shapes and sizes of the precipitates is essential for understanding the extent of strengthening. Indeed, there are many experimental studies of shape versus size of Al–Zn precipitates [12–21] using electron microscopy [transmission electron microscopy (TEM), high-resolution electron microscopy (HREM)] [12–15, 18], small-angle neutron scattering (SANS) [16], X-ray diffuse scattering (XDS) and small-angle X-ray scattering (SAXS) [13, 20, 21]. Experimental studies of precipitates in Al–Zn exhibit a broad series of coherent face-centered cubic (fcc) shapes, including spherical Guinier–Preston zones [2, 10], ellipsoidal and partially coherent platelets (with coherency along [111]) [13, 15, 17–19]. These results, summarized in Fig. 1, agree on the following points.

1. The precipitates show a deterministic shape versus size relation: very small precipitates possess a more spherical shape ($c/a \approx 1$ in Fig. 1) until they reach a critical radius of about 15–25 Å. Then, as

---

* To whom all correspondence should be addressed.

1359-6454/00/$20.00 © 2000 Acta Metallurgica Inc. Published by Elsevier Science Ltd. All rights reserved.
PII: S1359-6454(00)00209-3

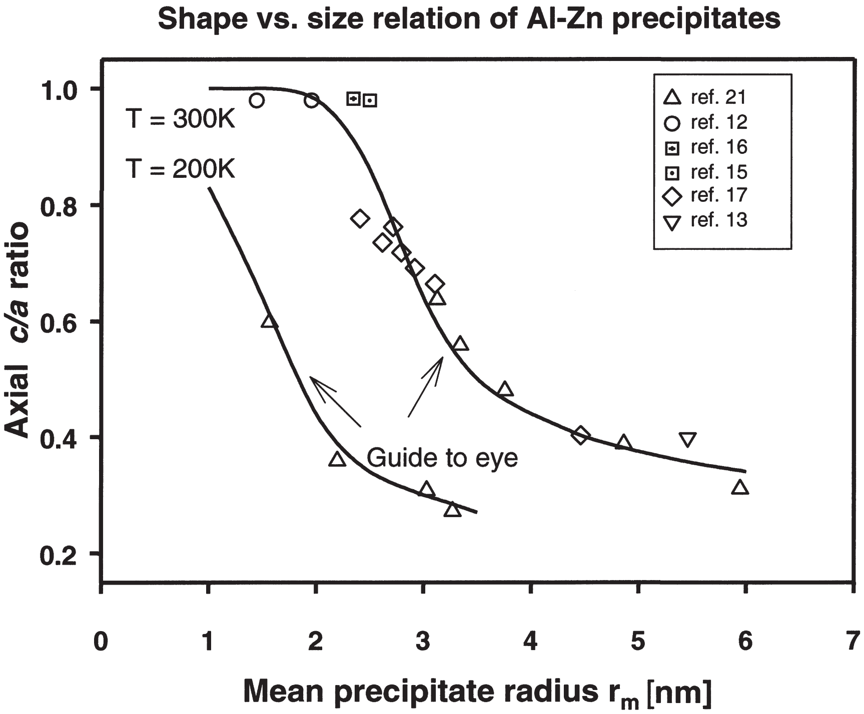

Fig. 1. Experimentally observed size versus shape relation in Al–Zn at room temperature (RT). Data are taken from different references (given in the figure). $r_m = (ca^2)^{1/3}$ is the radius of the associated sphere having the same volume as the corresponding precipitate.

the size increases, they become more ellipsoidal (smaller c/a values).

2. The precipitates show a shape versus temperature relation: in general, the transition from the nearly spherical shape into the more ellipsoidal shape occurs at smaller precipitate sizes the lower the applied aging temperature.
3. The ellipsoidal precipitates always have their short axis parallel to the [111] direction.

The last feature allows the definition of a c/a ratio and, therefore, a quantitative measure for the description of the precipitate shape: while a represents the long axis of the ellipsoid (perpendicular to [111]), c is its thickness (parallel to [111]). The size is given by $r_m = (ca^2)^{1/3}$, denoting the radius of the associated sphere having the same volume as the corresponding precipitate.

Although these experiments use completely different aging times, the distribution of points in Fig. 1 is deterministic; i.e., for a fixed aging temperature, the c/a ratio for a given precipitate size has a unique value. For samples aged at room temperature the ratio c/a is nearly 1 up to about $r_m = 2$ nm. Then, the c/a ratio starts to decrease until it reaches a value of about 0.3 at $r_m = 6$ nm. For a given size r_m, c/a can only be changed by lowering the aging temperature: the lower the aging temperature, the smaller is the resulting c/a ratio. This observation leads to the conclusion that the size–shape relation of precipitates does not depend on the aging time within experimental accuracy and, therefore, is *not controlled by kinetics*. Atomistically, this means that each individual precipitate represents a local equilibrium configuration. This is because atoms in a given precipitate exchange much faster with each other than with the other precipitates. Consequently, a theoretical model for describing the shape versus size and temperature relation in precipitates can be based on *thermodynamics*.

In principle, one could determine the shape versus size versus temperature of a precipitate if one optimizes the free-energy $F(r_m; T)$ of a given size r_m at a given temperature T with respect to all possible shapes. Technically, if one knew how the formation enthalpy $\Delta H(\sigma)$ depends on the configurational variable σ, this could be done via Monte-Carlo simulation of an alloy box at a given $(r_m; T)$. The most detailed way to describe configurational variables is atomistic; e.g., a configuration σ is a list of "spin variables" $\{\hat{S}_i, i = 1, \ldots, N\}$ denoting whether site i is occupied by an A atom ($S_i = -1$) or a B atom ($S_i = +1$). Thus, the problem is to determine the function $\Delta H_f(\sigma)$. Again, in principle, this can be done quantum-mechanically; i.e., evaluate

$$\Delta H_f(\sigma) = E_{tot}(\text{alloy}; \sigma) - xE_A^{tot}(a_A) - (1 - x)E_B^{tot}(a_B), \qquad (1)$$

where $E_{tot}(\text{alloy}; \sigma) = \langle\Psi|\hat{H}(\sigma)|\Psi\rangle/\langle\Psi|\Psi\rangle$ and $\hat{H}$ is the system's Hamiltonian. E_{A}^{tot} and $E_{B}^{\mathrm{tot}}(a_B)$ are the total energies of bulk elements A and B at the equilibrium lattice constant a_A and a_B, respectively. While this plan is straightforward, most previous approaches to this problem have used instead a highly simplified, non-quantum-mechanical model of $\Delta H_f(\sigma)$ (note, however, Refs. [22, 23]). The simplifications are centered around truncating the range of pair interactions [20], using macroscopic quantities to define "effective" atomistic quantities [24, 25], or applying continuum approaches in the context of empirically parametrized free-energy functionals [3, 26, 27]. As an example, Lee [28] used an interfacial energy that is independent of local strain and crystallographic orientation for his studies of the coherency strain via a discrete atom method. In this model, the interfacial energy of each interface atom is defined by its number of unlike bonds. For an interface, e.g., in the [111] direction (three unlike neighbors per atom) and in the [110] direction (i.e., an interface parallel to the [111] plane), the difference in the resulting interfacial energy is given by a factor of 1.29. However, our calculation of the interfacial energies for different directions at $T = 0$ using our model based on the local-density approximation (LDA) gives a 6.30 times larger interface energy for [110] than for [111] interface atoms. Moreover, we see a strong orientation dependence of the interfacial energy; i.e., small precipitates cannot be correctly described by a constant value for the interfacial energy. This example makes it clear that a quantum-mechanical approach is essential for describing precipitate shapes in systems which show a strong anistropy in the interfacial energy. An earlier quantum-mechanical study for the Al–Li system used a well-defined model supercell for the matrix–precipitate interface to predict the matrix–precipitate interfacial free-energy [29], but this ansatz does not allow a study of the complete shape of a precipitate, sometimes consisting of many thousands of atoms. Another access for theoretical studies of precipitates are fitting procedures, e.g., analyses of small-angle scattering patterns by non-linear fitting to a theoretical scattering curve based on a hard-sphere liquid model [30, 31]. These studies always need experimental input data and the particle shape found always represents an average, and does not give the shape of an individual precipitate. Earlier theoretical investigations by Khachaturyan and co-workers [32, 33] have shown (by use of a two-dimensional model) that the equilibrium shape of a precipitate at a given volume is determined by a balance between chemical free-energy (related to the inhomogeneous composition distribution) and the elastic energy. Recently, Rubin and Khachaturyan [24] investigated the dynamics and morphology of coherent microstructures in Ni–Al alloys. Separating the free-energy into a stress-free part and the elastic energy, they concluded that the observed [100] faceting of precipitates in Ni–Al is caused by strain. For their three-dimensional model they took necessary input parameters like crystal lattice misfit and elastic moduli from different experimental measurements (see references in Ref. [24]).

In contrast to empirical methods, our group has developed instead a fully atomistic, quantum-mechanical formulation of $\Delta H(\sigma)$ which is both accurate (being based on first-principles calculations) and fast (so it can be used in Monte-Carlo simulations). It not only includes anisotropies in the interfacial energies, but also takes inhomogeneous elastic energies as well as anharmonic elasticity into consideration [34]. The idea is to expand $\Delta H(\sigma)$ linearly into a sum of energies characteristic of atomic figures such as pairs, triangles, tetrahedra, and determine these energies from a set of first-principles calculations on prototype ordered compounds. This *Linear Expansion in Geometric Objects* approach [35] has been already applied to predict the $T = 0$ ground-state structures of many alloy systems [36, 37], the finite-temperature enthalpy and short-range order of alloys [38–41], and recently the precipitate shapes in Al–Cu [22] and Al–Mg [23].

In the present paper, we shall show that precipitate shape versus size versus temperature in Al–Zn alloys (Fig. 1) can be correctly described using this quantum-mechanical *parameter-free* model.

The paper is organized as follows. First (Section 2), the theoretical model is introduced and the theoretical procedure explained. Next (Section 3), our calculated precipitate shapes are compared with experimentally observed forms of precipitates as a function of size and temperature. In Section 4, we describe how the [111] "flattening" of precipitates is correlated with a mechanical instability of fcc Zn. Furthermore (Section 5), it is shown how the size versus shape relation at $T = 0$ K can already be explained qualitatively by energy calculations for simple model precipitates. Finally (Section 6), we discuss the size versus shape versus temperature relation by separating the total energy into physically motivated pieces such as strain and chemical energy.

2. THEORETICAL MODEL AND CONCEPTS

The basis of our approach is a *mixed-space cluster expansion* [35, 42], known as *Linear Expansion in Geometric Objects*. It allows one to calculate the formation enthalpy $\Delta H_f(\sigma)$, equation (1), of any arbitrary atomic configuration–even those consisting of more than 100,000 atoms—including energy lowering due to relaxations. Formulation of the method requires $T = 0$ formation enthalpies of 20–30 ordered compounds A_pB_q consisting of *only 2–16 atoms* per unit cell. The *formation enthalpy* $\Delta H_f(A_pB_q, \sigma)$ of such ordered A_pB_q bulk compounds is defined as the energy gain or loss with respect to the bulk constituents at their equilibrium lattice constants:

$$\Delta H_f(A_pB_q; \sigma) = E^{\mathrm{tot}}(A_pB_q, \sigma) - xE_A^{\mathrm{tot}}(a_A) - (1-x)E_B^{\mathrm{tot}}(a_B). \tag{2}$$

Here, σ denotes the type of ordered structure, and a_A and a_B are the equilibrium lattice constants of the bulk elements A and B. $E_A^{\mathrm{tot}}(a_A)$ and $E_B^{\mathrm{tot}}(a_B)$ are the total energies of A and B, respectively. The formation enthalpies of such small unit-cell structures can be easily calculated within the local-density approximation (LDA) [43–48]. In this very successful approximation, the energy density is approximated by the corresponding expression of the *homogeneous* electron gas with the replacement of the constant density n_0 by the local density $n(r)$ of the actual *inhomogeneous* system. The pseudopotential method was applied for the calculations [49, 50]. We used pseudopotentials of Troullier–Martins type [51] in the Kleinman–Bylander form [52]. They were carefully tested and successfully applied in an earlier Al–Zn study [41].

The mixed-space cluster expansion (CE) is an efficient and accurate method for calculating ground states, mixing enthalpies, superlattice energies, phase diagrams, short-range order (see, e.g., Refs. [34, 37, 40]) and, recently, precipitates [22, 23]. Any configuration σ is defined by specifying the occupations of each of the N lattice sites by an Al atom ($\hat{S}_i = -1$) or a Zn atom ($\hat{S}_i = +1$). The formation enthalpy of any configuration σ is then given by

$$\Delta H_{\mathrm{CE}}(\sigma) = \sum_{\boldsymbol{k}} J_{\mathrm{pair}}(\boldsymbol{k}) |S(\boldsymbol{k}, \sigma)|^2 + \sum_{f}^{MB} D_f J_f \bar{\Pi}_f(\sigma) + \frac{1}{4x - 1} \sum_{\boldsymbol{k}} \Delta E_{\mathrm{CS}}^{\mathrm{eq}}(\hat{k}, x) |S(\boldsymbol{k}, \sigma)|^2. \quad (3)$$

The first term includes all pair figures, where $J_{\mathrm{pair}}(\boldsymbol{k})$ and $S(\boldsymbol{k}, \sigma)$ are lattice Fourier transforms of real space interactions and spin-occupation variables. The second sum represents many-body interactions and runs over symmetry-inequivalent clusters consisting of three or more lattice sites. D_f is the number of equivalent clusters per lattice site, and $\bar{\Pi}_f(\sigma)$ are structure-dependent geometrical coefficients. The last summation involves the *constituent strain energy*, $\Delta E_{\mathrm{CS}}^{\mathrm{eq}}$, which is defined as the strain energy of bulk Al and fcc Zn required to maintain coherency along an interface with orientation $\hat{k}$. $\Delta E_{\mathrm{CS}}^{\mathrm{eq}}$ can be calculated by deforming the bulk elements (Al and fcc Zn) from their equilibrium lattice constants a_{Al} and a_{Zn} to a common lattice constant a perpendicular to $\hat{k}$.

Our formalism does not obtain the interaction energies from small-amplitude waves as done in Ref. [3], but, instead, we use LDA total energies of ordered structures (i.e., large concentration waves) for fitting the expansion. Also, unlike earlier models using the Landau stress-free free-energy functional [24, 33]: (1) our model includes explicitly all chemical interactions (e.g., charge transfer) and a large number of pair and multibody interactions, which is necessary for a detailed quantitative description of experimentally observed physical properties; and (2) the model is *parameter-free*, i.e., no experimental results are used as input parameters.

For finite-temperature studies, the CE Hamiltonian is combined with Monte-Carlo (MC) simulation based on the Metropolis algorithm. We used the canonical ensemble with fcc lattices containing from 27,000 up to 216,000 atoms. The model was recently applied to calculate the coherent fcc miscibility gap in Al–Zn by annealing the solid solution, lowering the temperature, and looking for the temperature at which the specific heat shows a maximum [41]. The ability to correctly predict the coherent fcc miscibility line in the phase diagram represents an important prerequisite for the precipitate studies. The coherent phase boundary is depressed below the incoherent miscibility gap due to the elastic strain associated with maintaining coherency between precipitate and matrix [53–55]. Experimental measurements of the top of the coherent miscibility gap from direct measurement techniques, such as X-ray diffraction, TEM studies and neutron scattering studies [56–58], give values from 318 to 328°C for compositions of about 37–40% Zn in good agreement with our calculations ($T_{\mathrm{C}} = 295$°C for 40% Zn; for details, see Ref. [41]). Precipitate shapes were calculated for precipitates consisting of $N_{\mathrm{Zn}} = 272$ up to $N_{\mathrm{Zn}} = 11{,}656$ Zn atoms in the following way. A large enough (see below) Monte-Carlo cell is chosen to guarantee that the precipitate shape formed is not influenced by the cell boundaries. We used periodic boundary conditions with the constraint that boundary sites are always occupied by Al atoms. These atoms are "frozen", i.e., cannot flip their identity. This restriction has the advantage that precipitates cannot grow over the cell boundaries. The number of sites in the cell and the chosen number of Zn atoms, N_{Zn}, automatically define the composition x of the alloy $\mathrm{Al}_{1-x}\mathrm{Zn}_x$. The critical temperature $T_{\mathrm{C}}(x)$, where the precipitation of Zn occurs, is known from our earlier calculated coherent phase boundary [41]. Starting from a random configuration for $\mathrm{Al}_{1-x}\mathrm{Zn}_x$ at a temperature well above the coherent phase boundary, the precipitate is formed by MC annealing to temperatures below the coherent phase boundary. At the end of the simulation all precipitates coalesce into one precipitate representing the equilibrium configuration for a given temperature and concentration. Typically, the temperature is lowered in 10 K steps. It is essential to ensure that the shape of the precipitate does not depend on the selected size of the MC cell. For *every* chosen number of Zn atoms N_{Zn}, the independence of precipitate shape at $T \rightarrow 0$ K resulting from MC annealing on the cell size was tested by using different MC cells. As an example, Fig. 2 compares the resulting shapes of a precipitate containing $N_{\mathrm{Zn}} = 2175$ atoms, using two different MC cells ($30 \times 30 \times 30$ and $40 \times 40 \times 40$). We see that the two shapes possess practically the same c/a ratio.

Fig. 3 illustrates the results of our MC simulation

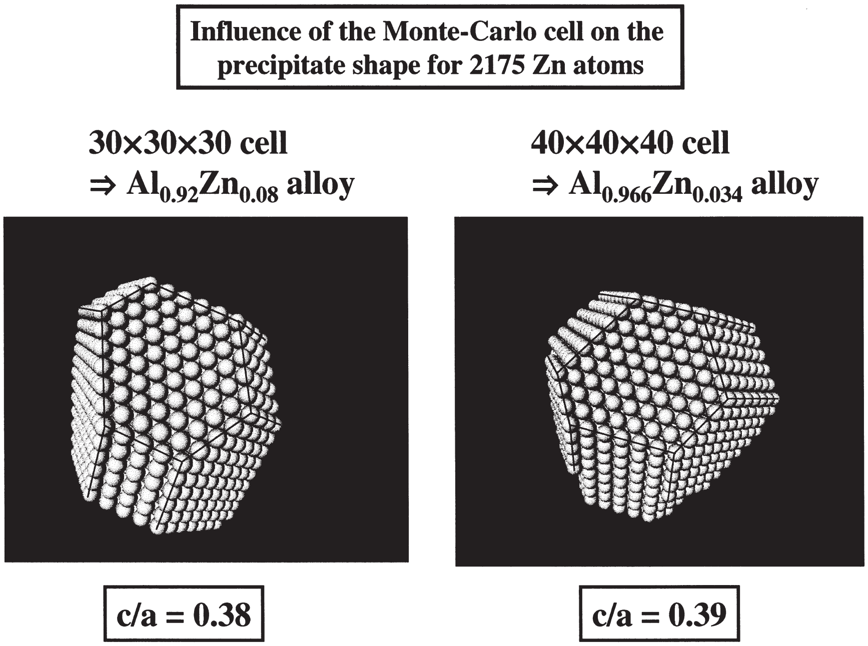

Fig. 2. Dependence of the equilibrium precipitate shape on the size of the Monte-Carlo cell (only Zn atoms are shown).

of an $Al_{0.966}Zn_{0.034}$ alloy containing $N_{Zn} = 918$ Zn atoms as a function of temperature (only Zn atoms are shown). We start from a temperature far above (here, $T = 2T_C$) the critical temperature T_C to ensure presence in the solid solution of the phase diagram. The equilibrium configuration at this temperature represents a disordered alloy. The precipitate is formed during annealing below T_C, until for $T \rightarrow 0$ all Zn atoms are part of the formed precipitate.

3. EQUILIBRIUM SHAPES OF PRECIPITATES

Applying the concept described in Section 2, we calculated the shapes of precipitates in Al–Zn for different numbers of Zn atoms. Fig. 4 shows a selection of precipitates for different temperatures below T_C and different sizes. It can be seen that: (1) precipitates become more ellipsoidal/hexagonal and well-ordered with decreasing temperature; (2) precipitates flatten with increasing size; and (3) the short axis is parallel to the [111] direction. This is visible best in the middle bottom picture. This preferred orientation can be interpreted as a consequence of two effects: a mechanical instability of fcc Zn and a strong anisotropy of the chemical energy of the system as discussed below in Section 4.

For a quantitative comparison of calculated and experimental shapes, we determined the c/a ratios of precipitates (c and a are shown schematically in the bottom right picture of Fig. 4). This determination allows a calculation of the mean radius $r_m = (ca^2)^{1/3}$. The experiment versus theory comparison of the resulting c/a ratios as function of r_m is shown in Fig. 5 for two different aging temperatures ($T = 300$ K and $T = 200$ K). The theoretical results are given by solid lines. For both temperatures, the agreement between our simulations and experimental measurements is excellent. This demonstrates the predictive power of our *thermodynamic* model in describing the size versus shape versus temperature relation of precipitates in Al–Zn.

4. WHY ARE THE AL–ZN PRECIPITATES ELONGATED ALONG [111]?

The experimentally observed and predicted (Fig. 4) "flattening" in [111] can be interpreted as a consequence of an unusual instability of fcc Zn. Fig. 6 compares the LDA-calculated total energies of fcc Zn that is uniaxially distorted along the [100] and [111] directions. The calculation is volume-conserving; i.e., the in-plane lattice constants a are varied, while the third lattice constant c is chosen so as to maintain the constant volume of the undistorted unit cell. Here, $c/a = 1$ represents the undistorted fcc state. We see that distortions along the [100] direction have an energetic minimum at $c/a = 1$ (the ideal fcc cell), distorting fcc Zn in the [111] direction leads to a new minimum around $c/a = 1.15$ lying -5.5 meV *below* the energy level of the ideal undistorted fcc Zn unit cell. Thus, unlike other fcc-based Al alloys (like Al–Cu), in Al–Zn the [111] direction is the elastically softest direction over the whole concentration regime. Besides the strain, the formation enthalpy of any configuration is controlled by the chemical nature of the atoms, as will be discussed in Section 6. As we have shown earlier [41], for Al–Zn the chemical energy shows a strong anisotropy, being lowest for the

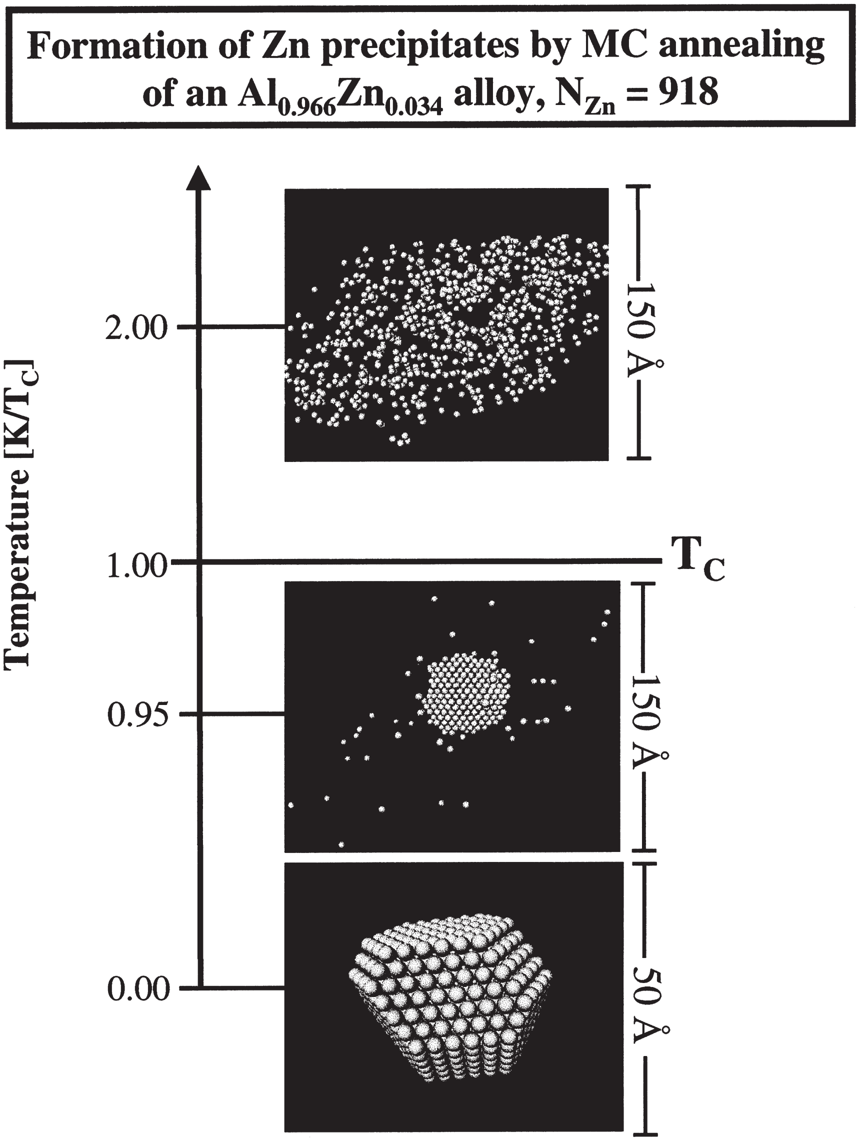

Fig. 3. Equilibrium configurations of an $Al_{0.966}Zn_{0.034}$ alloy from Monte-Carlo simulations above and below T_C, only Zn atoms are shown. Starting from a random configuration the Zn precipitate ($N_{Zn} = 918$) is formed during careful annealing below the critical temperature $T_C(x)$ given by the coherent fcc miscibility gap.

ordered Al_pZn_q compounds whose layers are oriented along the [111] direction. Consequently, we find [41] that such [111] superlattices show unusually stable formation enthalpies. For example, the Al_3Zn_3 superlattice along [111] has a formation enthalpy of only $\Delta H_f = +2.8$ meV/atom [41], while [001]-oriented structures are much higher in energy. The consequence for the formation of precipitates is now obvious: in no direction other than [111] are deformations so low in energy. Therefore, the "flattening" of precipitates in the [111] direction evident in Fig. 4 is caused by the extremely small [111] strain in Al–Zn in combination with a strong anisotropy of the chemical energy.

It is noteworthy that the *c*/*a* ratio (with respect to ideal close packing) at which the fcc Zn total energy has a minimum is practically identical to the *c*/*a* ratio in hexagonal close-packed (hcp) Zn (shown in Fig. 6 as a hexagon). Experimentally, hcp Zn has an anomalously large *c*/*a* ratio of 1.15 (with respect to ideal close packing). This anomaly of hcp Zn has been the subject of a number of earlier investigations (e.g., Refs. [59, 60]). The observation of the large *c*/*a* value in fcc Zn (Fig. 6) suggests that the physical mechanism that is responsible for the anomalous *c*/*a* ratio of hcp Zn could be the same as that causing the instability of fcc Zn. A detailed discussion about the instability of fcc Zn can be found in Ref. [41].

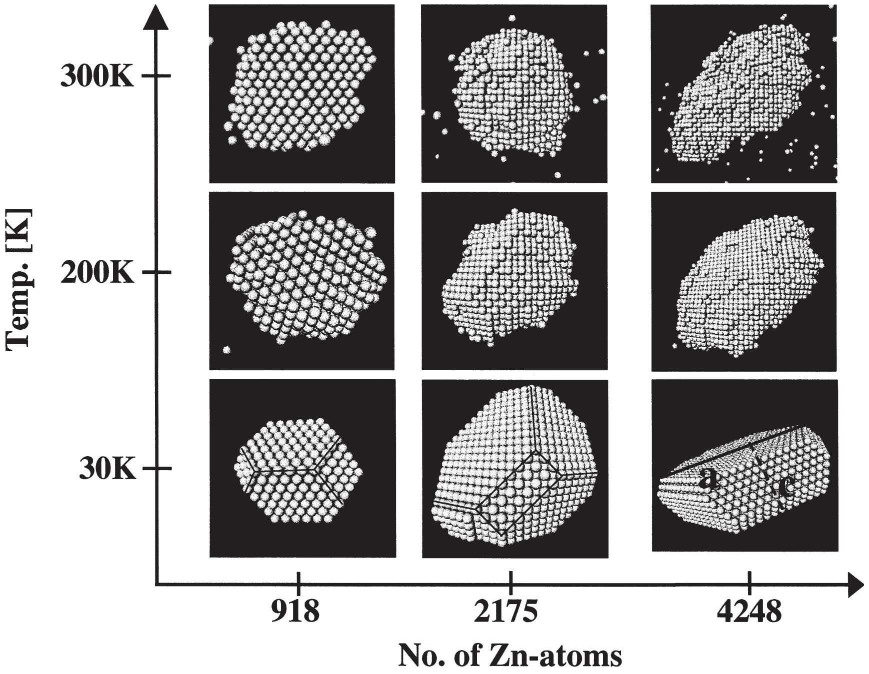

Fig. 4. Dependence of calculated coherent fcc Zn precipitate shape on the number of Zn atoms and temperature in Al–Zn alloys. The bottom right marks the *c*- and *a*-axes of the precipitate, which can be used for a quantitative comparison to experimental data (only Zn atoms are shown).

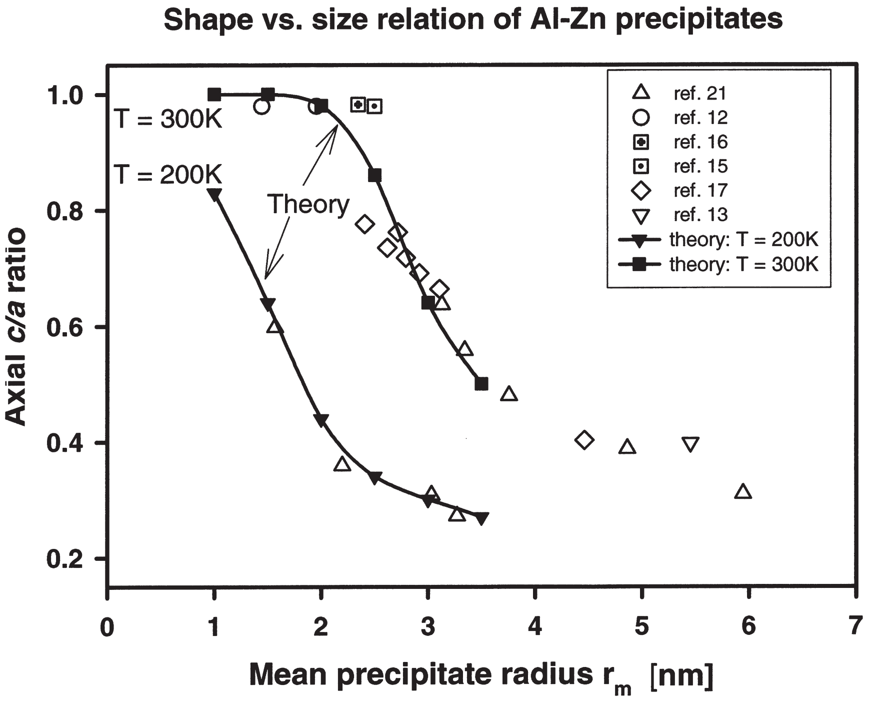

Fig. 5. Comparison of size versus shape relation of precipitates in Al–Zn between our calculations and experimental results for two different temperatures. $r_m = (ca^2)^{1/3}$ is the radius of the associated sphere having the same volume.

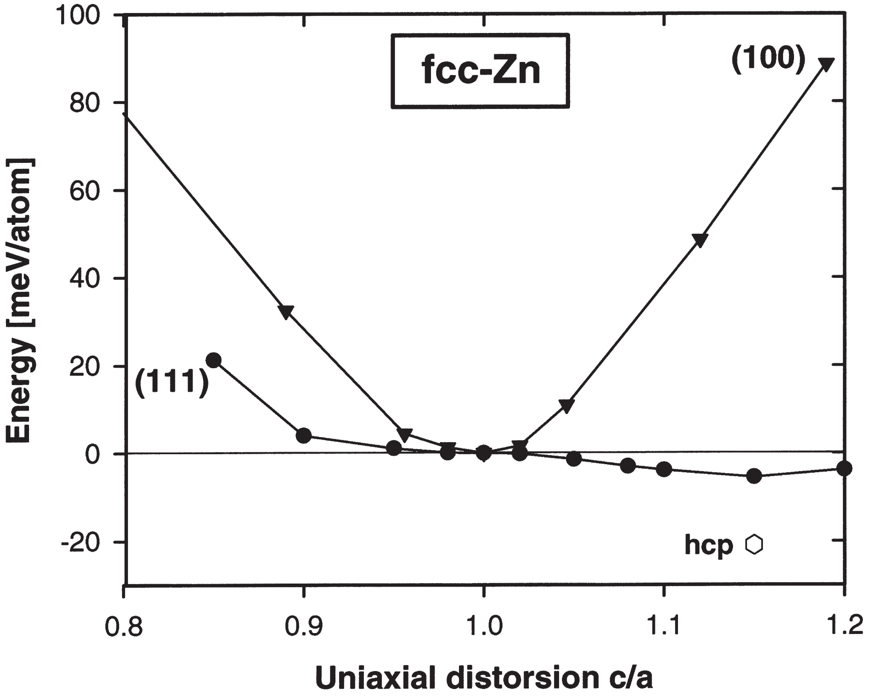

Fig. 6. Volume-conserving first-principles total energy calculations of fcc Zn deformed along the (100) and (111) directions. The energy differences caused by distortions along (100) and (111), as well as for hcp Zn, are always given with respect to the undistorted fcc lattice. The energy of hcp Zn is denoted as an open hexagon.

5. PHYSICAL ANALYSIS OF THE COMPUTATIONAL RESULTS

In order to shed light on the predicted size-dependent precipitate shape, we construct model precipitates with a *given* shape, c/a, and then evaluate their energy as function of size. Naturally, our cluster expansion Hamiltonian H_{CE} of equation (3) allows the calculation of any arbitrary given configuration at $T = 0$ K, i.e., *without* any Monte-Carlo simulations. The advantage of such an inverse approach is that the calculated energies of given shapes isolate the influence of the shape change on the energy, while the MC simulation changes the shape and the degree of order (i.e., disorder caused by finite temperature) *at the same time*, thus not allowing the effects to be separated. We chose the ideal sphere ($c/a = 1$), as well as hexagons with varying c/a ratios of 0.85, 0.50 and 0.35, as model precipitates for our calculations and determined their $T = 0$ energies for different numbers N_{Zn} of Zn atoms. The model precipitates are embedded in a $40 \times 40 \times 40$ fcc lattice cell. All sites that are not occupied by the Zn atoms, are occupied by Al atoms. So, the total number of atoms of any configuration is always 64,000. It should be mentioned that such a calculation of a formation enthalpy for a configuration consisting of 64,000 atoms does not take longer than a few seconds on a workstation or a modern PC. This short computer time for—in an atomistic sense—huge systems makes our cluster expansion a powerful tool.

Fig. 7 shows the dependence of the $T = 0$ energy of the four chosen model precipitates on their size. Only for extremely small precipitates (less than about 90 Zn atoms) does the ideal sphere ($c/a = 1.0$) represent the lowest energy at $T = 0$. With increasing size, the lowest-energy c/a ratio decreases, until at about 1600 Zn atoms the model with $c/a = 0.35$ becomes the energetically favorable shape. The transition points of the energy curves belonging to different c/a ratios are denoted in Fig. 7 by arrows. This calculation can be used to construct a step function in the size versus shape diagram, which we show in Fig. 8. For comparison, the size versus shape curve obtained via MC annealing for $T \to 0$ is also shown. It can be seen that the $T = 0$ energies of the model precipitates with given ratio c/a already predict qualitatively the observed size–shape relation: c/a becomes smaller with increasing size. It should be emphasized that the models chosen in Fig. 7 are assumed models and *do not* represent equilibrium configurations like the precipitates calculated from MC simulations (Figs. 2–5). However, these model precipitates clearly show that the observed size-dependent shape of precipitates can be already explained in terms of $T = 0$ energies.

6. SHAPE-CONTROLLING FACTORS: CHEMICAL AND STRAIN ENERGY

Until now, the energy of precipitates was always studied by considering the *full* cluster expansion

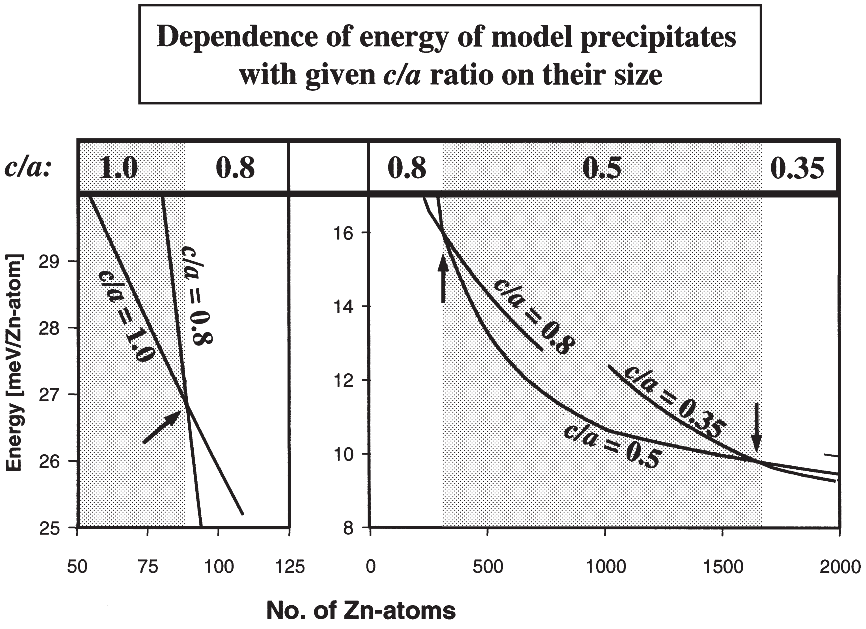

Fig. 7. $T = 0$ energy of precipitate models with *assumed* c/a value and number of Zn atoms, as obtained from the cluster expansion.

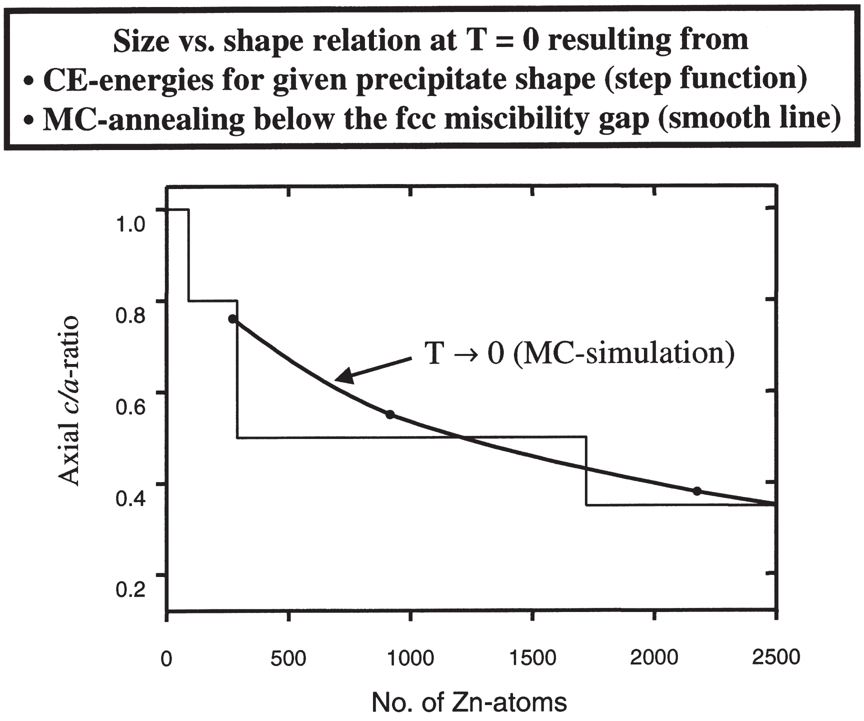

Fig. 8. Size versus shape step function resulting from the energies in Fig. 7, and comparison with the size versus shape dependence for $T \to 0$ K from Monte-Carlo simulations.

Hamiltonian of equation (3). This does not show which part of the H_{CE} controls the shape versus size and temperature relation. Next we separate our cluster expansion Hamiltonian into two parts, namely the *chemical energy* E_{chem} containing all pair and multibody interactions (and, therefore, the chemical nature of the alloy system) and the *strain energy* E_{CS}:

$$\Delta H = E_{chem}(\sigma) + E_{CS}(\sigma). \qquad (4)$$

The physical picture is as follows. We imagine forming a precipitate in two steps. First, we allow only strain energies to come into play. The energy functional of the strain is

$$E_{\mathrm{CS}}(\sigma) = \frac{1}{4x-1}\sum_{\boldsymbol{k}}\Delta E^{\mathrm{CS}}_{\mathrm{eq}}(\hat{k}, x)|S(\boldsymbol{k}, \sigma)|^2. \qquad (5)$$

As described in Section 2, $\Delta E^{\mathrm{eq}}_{\mathrm{CS}}$ can be calculated by the energy change caused by deformation of the *pure* bulk elements Al and fcc Zn in well-defined directions for a common lattice constant a. Consequently $\Delta E^{\mathrm{eq}}_{\mathrm{CS}}$, and therefore $E_{\mathrm{CS}}(\sigma)$, does not include information about the strength of chemical interactions between Al and Zn atoms, but is a function of composition x and direction $\hat{k}$ only. Precipitate shapes calculated by considering only $E_{\mathrm{CS}}(\sigma)$ will therefore reflect the elastic properties of the alloy system. Second, we present the case where non-strain (pair and multibody) interactions to come into play:

$$E_{\mathrm{chem}}(\sigma) = \sum_{\boldsymbol{k}} J_{\mathrm{pair}}(\boldsymbol{k})|S(\boldsymbol{k}, \sigma)|^2 + \sum_{f}^{MB} D_f J_f \bar{\Pi}_f(\sigma). \quad (6)$$

This part includes all of the information about strength and importance of different chemical interactions characterized by effective cluster interactions J_{pair} and J_f. It does not consider the energy necessary to maintain coherency between the Al and fcc Zn matrix caused by the lattice misfit; i.e., the precipitate is able to maintain coherency with the Al matrix for any arbitrary precipitate size. Precipitate shapes calculated by considering only $E_{\mathrm{chem}}(\sigma)$ will therefore reflect the properties of the chemical interactions in Al–Zn. Naturally, this separation is not unique, but, as we shall see, it allows us to discuss and understand by which energetical factors the precipitate shape is controlled. It should be emphasized that an analogous decomposition of precipitate *shapes* corresponding to the two defined energy parts of the Hamiltonian is not possible because, unlike the energies, geometrical shapes are *not* additive.

For the following, a fixed precipitate size ($N_{\mathrm{Zn}} = 11{,}656$) was chosen. The Monte-Carlo cell consisted of $60 \times 60 \times 60 = 216{,}000$ atoms which defines the considered alloy as $\mathrm{Al}_{0.946}\mathrm{Zn}_{0.054}$. The MC annealing process was made for three different cases: (a) using only the consituent strain energy E_{CS}, (b) using only the chemical energy E_{chem}, and (c) using the full Hamitonian ΔH for the calculation. The resulting shapes for $T \rightarrow 0$ K are shown in Fig. 9. We see that the strain part [Fig. 9(a)] is platelet-stabilizing, while the "chemical part" [Fig. 9(b)] leads to a more spherical shape. The observed equilibrium shape [Fig. 9(c)] at $T = 0$ K will therefore be given by a (non-additive) combination of these two effects. Recently, similar results were found for atomistic calculations with a model Hamiltonian [23]. Furthermore, we see that the compact shape resulting from the calculation without the constituent strain, Fig. 9(a), possesses interfaces that are oriented in one of the four [111] directions. As mentioned Section 4, this preference is a consequence of a strong anisotropy of the chemical energy for Al–Zn (for details, see Ref. [41]). The described behavior is also known from earlier studies on different systems using the continuum approximation [3, 26, 27]. However, the continuum approximation is not able to describe atomistic features, and therefore is a good approximation only if interfacial area and precipitate size are sufficiently large (see also discussion in Section 1).

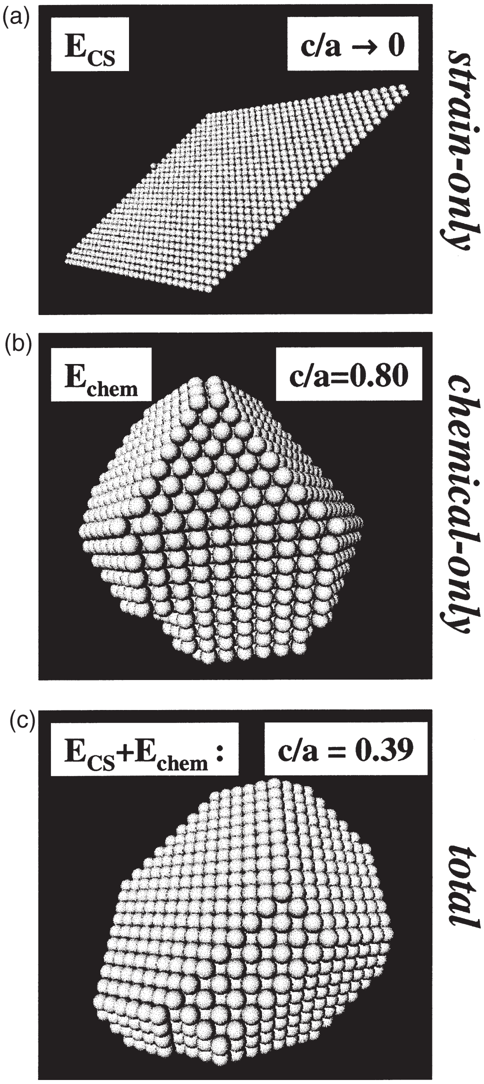

Fig. 9. Precipitate shape at $T \rightarrow 0$ K from Monte-Carlo calculations using (a) only the constituent strain energy E_{CS}, (b) only the "chemical" energy E_{chem} and (c) the full Hamiltonian $E_{\mathrm{CS}} + E_{\mathrm{chem}}$. While the strain part leads to a platelet, the chemical interactions promote a nearly spherical precipitate (only Zn atoms are shown).

The knowledge that different energy parts stabilize different characteristic shapes can be used to study the phase-stabilizing factors at *finite temperatures*. For this purpose, we stored the strain and chemical energy of equilibrium configurations obtained at different finite temperatures of the MC annealing process. Unlike the simulations leading to Fig. 9, the decomposition of the energy was always made *after* the MC simulation. The resulting energy curves for the total Hamiltonian ΔH, the chemical energy E_{chem} and the strain energy E_{CS} as function of temperature are shown in Fig. 10. Since the energy was separated after the simulation, for each temperature, the sum of chemical and strain energy must be equal to the total energy ΔH per Zn atom. We observe the following:

1. at high temperatures (> 150 K) the contribution of the chemical energy to the total energy is larger than the contribution of the strain energy, while the opposite is true for lower temperatures (< 150 K); and
2. while the chemical energy decreases strongly with decreasing temperature, the strain energy is nearly temperature-independent.

The temperature dependence of the two energy components becomes more obvious if we separate them into *temperature-dependent* and *temperature-independent* parts. For this, the CE Hamiltonian is written as

$$\Delta H = E_{\text{chem}}(N, T_C) + [E_{\text{chem}}(N, T) - E_{\text{chem}}(N, T_C)] + E_{\text{CS}}(N, 0) + [E_{\text{CS}}(N, T) - E_{\text{CS}}(N, 0)]. \tag{7}$$

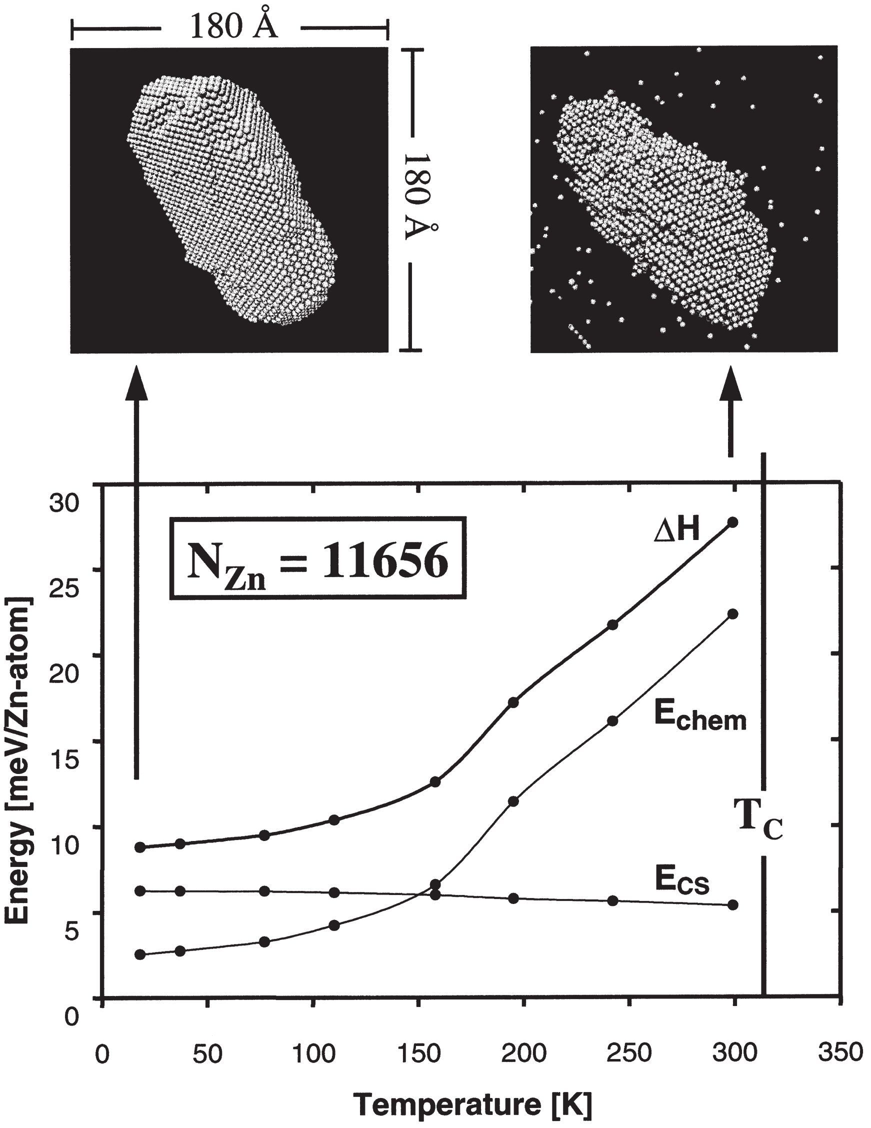

Fig. 10. Dependence of energy ΔH on temperature for a given precipitate size ($N_{\text{Zn}} = 11{,}656$). After annealing, the energy was decomposed into strain E_{CS} and chemical E_{chem} parts. While for temperatures higher than ~ 150 K the contribution of the chemical part to the total energy is larger than that of the strain part, the opposite is true for lower temperatures. For $T \to T_C$ and $T \to 0$ K the resulting precipitate shapes are shown (only Zn atoms are shown).

Here, $E_{\mathrm{chem}}(N, T_C)$ is the temperature-independent chemical energy of the precipitate (evaluated at $T \rightarrow T_C$), and $E_{\mathrm{CS}}(N, 0)$ is the temperature-independent strain energy of the precipitate (evaluated at $T \rightarrow 0$). The reason for this choice is that the chemical part is larger for $T \rightarrow T_C$, while the strain part is dominant for $T \rightarrow 0$. The two equilibrium shapes corresponding to $T \rightarrow T_C$ and $T \rightarrow 0$ are shown in Fig. 10. The energy terms of equation (7) are presented graphically in Fig. 11, where the two temperature-independent reference energies, $E_{\mathrm{chem}}(N, T_C)$ and $E_{\mathrm{CS}}(N, 0)$, are given as horizontal lines. This clearly demonstrates the strong temperature dependence of the chemical energy given by the shaded area between the reference energy $E_{\mathrm{chem}}(N, T_C)$ and the chemical energy $E_{\mathrm{chem}}(N, T)$. This observation is in excellent agreement with earlier theoretical studies [27, 29, 61] reporting a strong temperature dependence of interfacial energies. These investigations show that the anisotropy in interfacial energies is removed by configurational entropy which leads to a strong temperature dependence of the chemical energy and, therefore, to more spherical precipitates at high temperatures with faceting occuring at low temperatures.

7. SUMMARY

A cluster expansion approach known as *Linear Expansion in Geometric Objects* combined with Monte-Carlo simulations allows a theoretical description and understanding of the experimentally observed size versus shape versus temperature relation of precipitates in Al–Zn alloys. The simulation results also go through a quantitative comparison with experiment, the agreement is excellent. The precipitate shape shows a transition from a nearly spherical to a more ellipsoidal/hexagonal shape with *increasing size* and *decreasing temperature*. The "flattening" in the [111] direction can be interpreted as a combination of two effects: a recently found instability of fcc Zn when rhombohedrally distorted along [111] [41], and a strong anisotropy of the chemical energy. The size versus shape versus temperature relation can be decribed by *thermodynamics*; i.e., the relation does not depend on the growth conditions, but only on the size–shape distribution of precipitates: the longer the aging time, the more larger (and therefore) ellipsoidal the precipitates found in experimental studies [15].

$$\boxed{\begin{aligned} \Delta H = {} & E_{\mathrm{chem}}(N, T_c) + [\, E_{\mathrm{chem}}(N,T) - E_{\mathrm{chem}}(N,T_c)] \; + \\ & + E_{\mathrm{CS}}(N, 0) \quad + [E_{\mathrm{CS}}(N,T) - E_{\mathrm{CS}}(N, 0)] \end{aligned}}$$

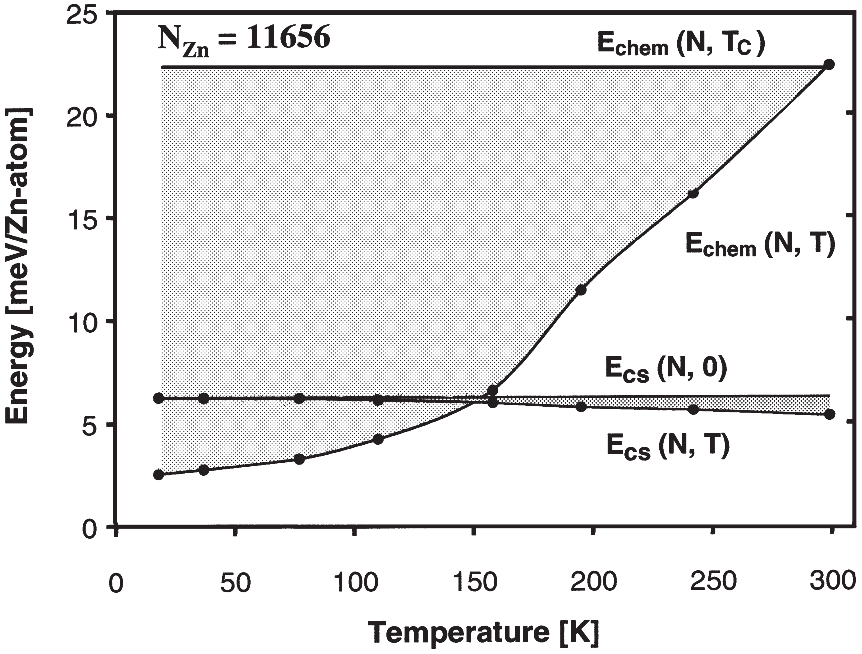

Fig. 11. Temperature dependence of chemical energy and strain energy ($N_{\mathrm{Zn}} = 11{,}656$). The dark and bright shaded areas give the deviation of the chemical and strain energy, respectively, from a chosen temperature-independent reference value. While the chemical energy shows a strong temperature dependence, the strain energy is nearly temperature-independent. The precipitate shapes of the chosen "reference" energies, $E_{\mathrm{chem}}(N, T_C)$ and $E_{\mathrm{CS}}(N, 0)$, are shown in Fig. 10.

The dependence of the shape on the size at $T = 0$ K can already be found by calculating energies for perfectly ordered model precipitates. We used an ideal spherical precipitate and hexagons with c/a ratios of 0.8, 0.5 and 0.35 for our calculations. These four model precipitates already give qualitatively, via Monte-Carlo simulations, the observed size versus shape relation: namely, a decreasing c/a ratio with increasing precipitate size.

The separation of the cluster expansion Hamiltonian into chemical and strain energy allows a deeper view inside the energetically controlled size versus shape relation. Monte-Carlo simulations only taking the chemical and strain energy into account lead, for $T = 0$ K, to different characteristic shapes for both energy parts: while the strain energy is platelet-stabilizing, the chemical part leads to a more spherical shape. Using this separation also for finite temperatures, it turns out that the shape versus size versus temperature relation for a given precipitate size is controlled by two different factors:

1. competition between strain and chemical energy—the chemical energy dominates over the strain part for higher temperatures, and the opposite is true for lower temperatures; and
2. temperature dependence of chemical energy—while the strain energy is nearly constant as a function of temperature, the chemical energy decreases strongly with decreasing temperature.

Since our model is parameter-free, the excellent agreement demonstrates the ability to predict precipitate shapes and sizes even without carrying out experiments.

Acknowledgements—The work at NREL was supported by the Office of Science, Basic Energy Science, Material Science Division, US Department of Energy, under Contract No. DE-AC36-99-GO10337.

REFERENCES

1. Guinier, A., *Solid State Phys.*, 1959, **9**, 293.
2. Cohen, J. B., *Solid State Phys.*, 1986, **39**, 131.
3. Khachaturyan, A. G., *Theory of Structural Transformations in Solids*. John Wiley, New York, 1983.
4. Gerold, V., *Scripta Metall.*, 1988, **22**, 927.
5. Mattila, T., Wang, L. -W. and Zunger, A., *Phys. Rev. B*, 1999, **59**, 15270.
6. Zunger, A. and Mahajan, S., chapter 19, in *Material, Properties, and Preparation*, ed. S. Mahajan, Handbook of Semiconductors, Vol. 3B, North Holland, New York, 1994, p. 1399.
7. Hansen, M., *Consitution of Binary Alloys.*, McGraw-Hill, New York, 1958.
8. Hultgren, R., Desai, P. D., Hawkins, D. T., Gleiser, M. and Kelley, K. K., *Selected Values of the Thermodynamic Properties of Binary Alloys.*, American Society for Metals, Metals Park, OH, 1973.
9. Massalski, T. B., in *Binary Alloy Phase Diagrams*, eds J. L. Murray, L. H. Bennett and H. Baker, American Society for Metals, Metals Park, OH, 1986.
10. Murray, J. L., *Bull. All. Ph. Diagr.*, 1983, **4**, 55.
11. Hatch, J. E., *Aluminum: Properties and Physical Metallurgy*. American Society for Metals, Metals Park, OH, 1998.
12. Laslaz, G. and Guyot, P., *Acta metall.*, 1977, **25**, 277.
13. Deguercy, J., Denanot, M. F., Fumeron, M., Guillot, J. P. and Caisso, J., *Acta metall.*, 1982, **30**, 1921.
14. Ramlau, R. and Löffler, H., *Phys. Stat. Sol. (a)*, 1981, **68**, 531.
15. Ramlau, R. and Löffler, H., *Phys. Stat. Sol. (a)*, 1983, **79**, 141.
16. Bubeck, E., Gerold, V. and Kostorz, G., *Cryst. Res. Technol.*, 1985, **20**, 97.
17. Hübner, G., Löffler, H. and Wendrock, G., *Cryst. Res. Technol.*, 1986, **21**, 8.
18. Gerold, V., Siebke, W. and Tempus, G., *Phys. Stat. Sol. (a)*, 1987, **104**, 213.
19. Guilarducci de Salva, A., P Simon, J., Livet, F. and Guyot, P., *Scripta metall.*, 1987, **21**, 1061.
20. Haeffner, D. R. and Cohen, J. B., *Acta. metall.*, 1989, **37**, 2185.
21. Fumeron, M., Guillot, J. P., Dauger, A. P. and Caisso, J., *Scripta metall.*, 1980, **14**, 189.
22. Wolverton, C., *Phil. Mag. Lett.*, 1999, **79**, 683.
23. Wolverton, C., *Model. Simul. Mater. Sci.*, 2000, **8**, 323.
24. Rubin, G. and Khachaturyan, A. G., *Acta mater.*, 1999, **47**, 1995.
25. Shneck, R., Brokman, A. and Dariel, M. P., *Phys. Rev. B*, 1992, **46**, 483.
26. Thompson, M. E., Su, C. S. and Voorhees, P. W., *Acta metall.*, 1994, **42**, 2107.
27. Lee, J. K., Barnett, D. M. and Aaronson, H. I., *Met. Trans. A*, 1977, **8A**, 963.
28. Lee, J. K., *Scripta metall.*, 1994, **32**, 559.
29. Sluiter, M. and Kawazoe, Y., *Phys. Rev. B*, 1996, **54**, 10381.
30. Triolo, R., Caponetti, E. and Spooner, S., *Phys. Rev. B*, 1989, **39**, 4588.
31. Floriano, M. A., Caponetti, E. and Triolo, R., *Phys. Rev. B*, 1992, **45**, 1016.
32. Wang, Y., Chen, L. -Q. and Khachaturyan, A. G., *Scripta metall.*, 1991, **25**, 1387.
33. Wang, Y., Wang, H., Chen, L. -Q. and Khachaturyan, A. G., *J. Am. Ceram. Soc.*, 1993, **76**, 3029.
34. Ozolins, V., Wolverton, C. and Zunger, A., *Phys. Rev. B*, 1998, **57**, 4816.
35. Zunger, A., in *Statics and Dynamics of Alloy Phase Transformations (NATO ASI)*, eds P. E. A. Turchi and A. Gonis, Plenum Press, New York, 1994, p. 361.
36. Lu, Z. W., Laks, D. B., Wei, S. -H. and Zunger, A., *Phys. Rev. B*, 1994, **50**, 6642.
37. Ozolins, V., Wolverton, C. and Zunger, A., *Phys. Rev. B*, 1998, **57**, 6427.
38. Wolverton, C., Zunger, A. and Lu, Z. -W., *Phys. Rev. B*, 1994, **49**, 16058.
39. Silverman, A., Zunger, A., Kalish, R. and Adler, J., *Phys. Rev. B*, 1995, **51**, 10795.
40. Wolverton, C., Ozolins, V. and Zunger, A., *Phys. Rev. B*, 1998, **57**, 4332.
41. Müller, S., Wolverton, C., Wang, L. -W. and Zunger, A., *Phys. Rev. B*, 1999, **60**, 16448.
42. Laks, D. B., Ferreira, L. G., Froyen, S. and Zunger, A., *Phys. Rev. B*, 1982, **46**, 12587.
43. Slater, J. C., *Phys. Rev.*, 1951, **81**, 385.
44. Zunger, A. and Freeman, A. J., *Phys. Rev. B*, 1977, **15**, 5049.
45. Zunger, A. and Freeman, A. J., *Phys. Rev. B*, 1977, **16**, 906.
46. Zunger, A. and Freeman, A. J., *Phys. Rev. B*, 1977, **16**, 2901.
47. Ceperley, D. M. and Alder, B. J., *Phys. Rev. Lett.*, 1980, **45**, 567.
48. Perdew, J. P. and Zunger, A., *Phys. Rev. B*, 1981, **23**, 5048.

49. Phillips, J. C. and Kleinman, L., *Phys. Rev.*, 1959, **116**, 287.
50. Cohen, M. L. and Heine, V., *Solid State Phys.*, 1970, **24**, 37.
51. Troullier, N. and Martins, J. L., *Phys. Rev. B*, 1991, **43**, 1993.
52. Kleinman, L. and Bylander, D. M., *Phys. Rev. Lett.*, 1982, **48**, 1425.
53. Cahn, J., *Acta metall.*, 1961, **9**, 795.
54. Cahn, J., *Acta metall.*, 1962, **10**, 179.
55. de Fontaine, D., *Solid State Phys.*, 1979, **34**, 73.
56. Simerska, M., Synecek, V. and Sima, V., *Czech. J. Phys. (C)*, 1974, **24**, 543.
57. Simerska, M. and Bartuska, B., *Czech. J. Phys. (C)*, 1974, **24**, 654.
58. Schwahn, D. and Schmatz, W., *Acta metall.*, 1978, **26**, 1571.
59. Singh, D. and Papaconstantopoulos, D. A., *Phys. Rev. B*, 1990, **42**, 8885.
60. Zheng-Johansson, J. X., Eriksson, O. and Johansson, B., *Phys. Rev. B*, 1999, **59**, 6131.
61. Asta, M., *Acta mater.*, 1996, **54**, 10381.